# Reports

## Observation of Single-Electron Charging in Double-Barrier Heterostructures

Bo Su, V. J. Goldman,* J. E. Cunningham

**Incremental single-electron charging of size-quantized states has been observed in the well in submicrometer double-barrier resonant tunneling devices. In order to distinguish between the effects of size quantization and the single-electron charging, the heterostructure material was grown asymmetrical so that one barrier is substantially less transparent than the other. In the voltage polarity such that the emitter barrier is more transparent than the collector barrier, electrons accumulate in the well; incremental electron occupation of the well is accompanied by Coulomb blockade, which leads to sharp steps of the tunneling current. In the opposite voltage polarity the emitter barrier is less transparent than the collector barrier and the tunneling current reflects resonant tunneling through size-quantized well states.**

Modern microfabrication techniques have been used to make metal-electrode tunnel junctions with capacitance $C$ small enough to observe single-electron charging effects (*1*). These effects arise when the elementary charging energy $U_C = e^2/2C$ of the junction is substantial so that the voltage needed to charge such capacitance by electronic charge $e$, $V_C = e/2C$, is observable. For biases $V < V_C$, tunneling of an electron is energetically unfavorable and the tunneling current is suppressed ("Coulomb blockade") (*2*). For biases $V > V_C$ tunneling is possible, and single-electron tunneling (SET) events are correlated (*3*). Single-electron charging has been also reported (*4*) in Si and GaAs "Coulomb islands" defined by gates in two-dimensional electron gas where, however, size quantization is negligible (*5*).

Microfabrication techniques have also been used to achieve "in-plane," lateral confinement of electronic states in semiconductor heterostructures that result in observable size quantization ("quantum dots") (*6*). Current-voltage (*I-V*) curves of submicrometer double-barrier resonant tunneling structures (DBRTS) show clear structure of multiple RT current peaks, which demonstrates tunneling through laterally quantized states in the well (*7–9*). As has been shown in (*10*), large-area DBRTS under bias contain $\sim 10^{10}$ cm$^{-2}$ electrons in the well so that a $10^{-5}$ cm diameter device would have just ~1 electron. In such devices, tunneling of a single electron can result in appreciable charging of the well so that the probability of tunneling of the next electron is drastically affected and tunneling of individual electrons through emitter and collector barriers is correlated in a manner similar to SET in metal double junctions (*11*).

We report the observation of single-electron charging of the well confined between two penetrable barriers in submicrometer DBRTS. In large-area DBRTS devices, electrons tunnel from emitter electrode to two-dimensional resonant states in the well; subsequently, electrons leave the well by tunneling through the collector barrier. The tunneling electrons are dynamically stored in the well to create a space-charge layer, which can strongly affect relative energy alignment of the well with respect to the emitter (*10*). The number of electrons in the well $N_W$ is proportional to the tunneling current $I$, $N_W = I\tau_W/e$, where $\tau_W$ is the lifetime in the well (both $I$ and $N_W$ are proportional to the area of the device). Since $I$, in turn, is determined by the relative energy alignment of the well and emitter, this feedback mechanism can lead to intrinsic bistability of a device instead of negative differential conductance (*10*).

In order to separate the charging and the size-quantization effects (as discussed below) we have used asymmetric DBRTS devices (*12*). The band diagrams of a large device are shown in Fig. 1. Under positive bias the emitter barrier is less transparent than the collector barrier, that is, $T_E << T_C$, where $T_E$'s and $T_C$ are transmission coefficients (which generally are bias dependent). Therefore the areal electron density in the well $n_W$ is relatively small. Under negative bias $T_E >> T_C$ and $n_W$ is quite considerable; the resulting negative feedback shifts the peak of the tunneling current to higher (in magnitude) bias and causes bistability. We determine the voltage dependences of $n_W(V)$, $T_E(V)$, $T_C(V)$, and so forth for both bias polarities by fitting experimental data of a large-area device with a generalization of the self-consistent DBRTS model described in (*10*).

Our DBRTS material was grown by molecular beam epitaxy. The active layer consists of a 9-nm GaAs well sandwiched between a 10-nm $Al_{0.34}Ga_{0.66}As$ barrier and an 11.5-nm $Al_{0.36}Ga_{0.64}As$ barrier (substrate side). The GaAs emitter and collector electrodes are Si-doped to $2 \times 10^{17}$ cm$^{-3}$. The wafer has a non-alloyed Al ohmic contact grown epitaxially in situ so that no heat treatment of the devices was needed. Devices of nominal diameters $D = 0.5$ to 3 μm were defined by electron beam lithography and wet chemical etching. As discussed elsewhere (*9*) the electrical size of devices $a$ is smaller than $D$ by ~350 nm because of etching undercut and surface depletion. Large devices exhibit peak-to-valley current ratio of >50:1 in the positive and intrinsic bistability in the negative bias, which indicates that our fabrication process does not induce device-quality degradation.

Measurements were done in a dilution refrigerator; temperatures were measured by a calibrated $Ru_2O_3$ chip resistor. The *I-V* characteristics of the devices were measured with a low-noise voltage-source biasing circuit. Similar results were obtained in several devices, although about one half of our small devices exhibited a different type of *I-V* curve, most likely due to the presence of a shallow donor in the well, as reported by Dellow *et al.* (*8*).

The *I-V* characteristics of a submicrometer device are shown in Fig. 2. The asymmetry of the two barriers is reflected in the asymmetry of the *I-V* curve with respect to the bias polarity. The positive-bias *I-V* curve has a peak current $I_p \approx 40$ pA. The *I-V* character-

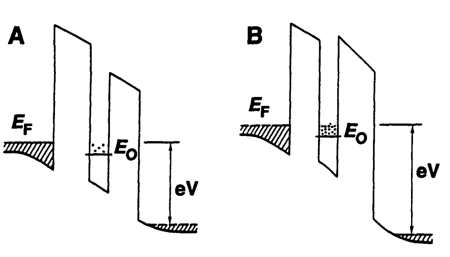

**Fig. 1.** Schematic energy diagrams of a large asymmetric DBRTS device under positive (**A**) and negative (**B**) bias. Hatching represents electron population of the emitter (left) and collector (right) electrodes; dots represent the electron population in the well. $E_0$ is measured from the bottom of the well to the bottom of the subband of the two-dimensional resonant states.

---

B. Su and V. J. Goldman, Department of Physics, State University of New York, Stony Brook, NY 11794–3800.
J. E. Cunningham, AT&T Bell Laboratories, Holmdel, NJ 07733.

---

*To whom correspondence should be addressed.

istics of the same device for negative bias with $I_p \approx 470$ pA is shown in Fig. 2B; Fig. 2C gives a blowup of this curve near threshold. The tunneling current is immeasurably small (<0.1 pA) in both polarities as the bias is increased from zero until the first step. The short period ($\sim$1 mV) modulation is quite reproducible and displays regular shifts with magnetic field; its origin is not clear at present. Most of the structure in the *I-V* curves washes out at a temperature of 15 K (Fig. 3).

Size quantization and single-electron charging are compatible and may coexist. For cylindrical DBRTS devices the charging energy $U_C = e^2/2C_W$, where the well capacitance $C_W \approx \varepsilon a^2/4\pi d$, is determined by the device diameter $a$, "effective barrier thickness" $d$, and material dielectric constant $\varepsilon$. The characteristic energy separation of the in-plane quantized levels $\delta E \approx \pi^2\hbar^2/2m^*a^2$ is determined by $a$ and by the effective mass in the well $m^*$. The ratio $U_C/\delta E \approx 4de^2m^*/\pi\varepsilon\hbar^2 \approx d/a_B$, where $a_B = 10$ nm is the GaAs effective Bohr radius, is independent of $a$. For $d = 10$ nm, $U_C/\delta E \approx 1$; thus, the single-electron charging should be observable in DBRTS devices when size quantization is observed and $d/a_B \geq 1$ *(13)*.

We proceed to consider tunneling current for a submicrometer DBRTS near $V_{th}$. At zero temperature, RT current through one state in the well is *(10, 14)*

$$I^{(1)} \approx (e/\hbar)[T_E E_F \cdot T_C E_0/(T_E E_F + T_C E_0)]$$

which takes into account the Pauli principle for occupation of the well states. The Coulomb blockade impedes tunneling until the first step in both bias polarities. In the positive bias, $T_E E_F << T_C E_0$, and every well state through which tunneling is energetically allowed is occupied only for a small fraction of time ($I^{(1)}$ is limited by the emitter barrier). Thus, after overcoming the Coulomb blockade, tunneling can proceed through several well states even when there is at most only one electron in the well at any given time. The first current step is equal to $2I^{(1)}$, the factor of 2 accounting for the spin degeneracy of the well state. As the bias is increased further, the current can increase, which reflects the greater number of the well states available for RT until it is energetically possible to have two electrons in the well at the same time. Thus, the *I-V* curve of Fig. 2A reflects SET through an increasing number of size-quantized well states.

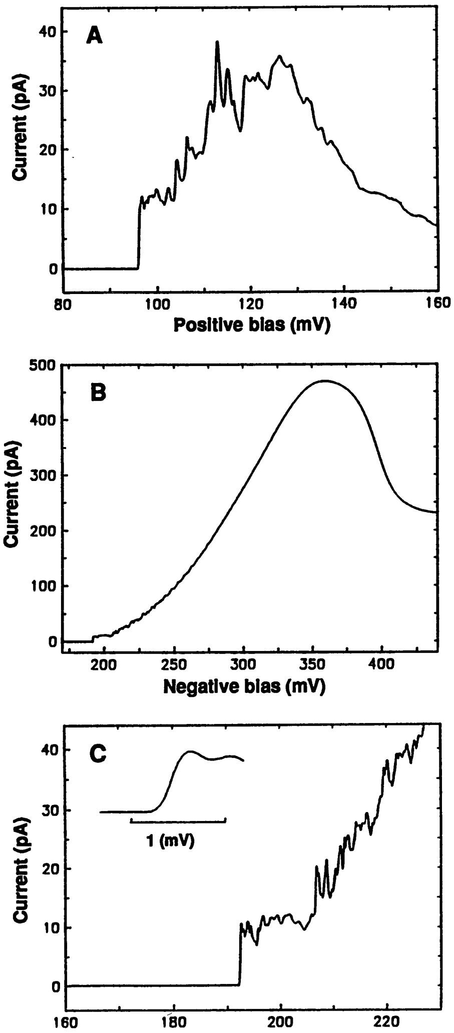

**Fig. 2.** Current-voltage curves of a submicrometer DBRTS device with nominal diameter (see text) $D = 0.5$ μm at 20 mK for (**A**) positive bias and (**B** and **C**) negative bias. The first sharp current step occurs when the Coulomb blockade for tunneling of a single electron into the well is overcome. (C) A blowup of (B) near threshold; the first current step is magnified in the inset.

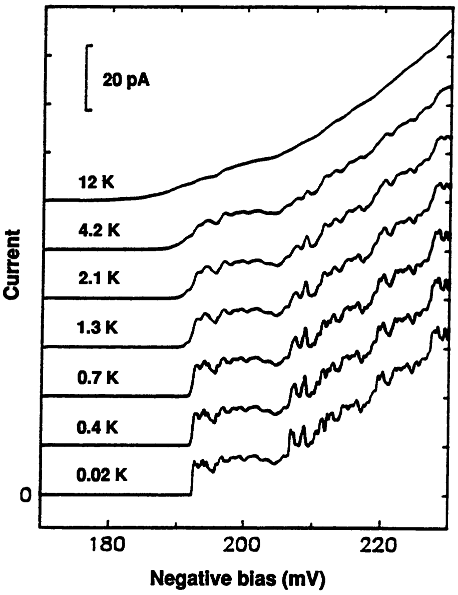

**Fig. 3.** Temperature dependence of the *I-V* curve near threshold.

In the negative bias, $T_E E_F >> T_C E_0$, and, after overcoming the Coulomb blockade, the lowest well state is occupied most of the time ($I^{(1)}$ is limited by the collector barrier). In contrast to the positive bias, under negative bias, even though the only tunneling electron can tunnel through several of the lowest well states, after the first current step the current stays nearly constant until it is energetically possible to have two electrons in the well at the same time, when the second step occurs (Fig. 2C).

This interpretation is supported by the magnetotunneling data (with magnetic field $B$ perpendicular to the barriers) (Fig. 4). In the positive bias the first current step occurs when the Coulomb blockade for tunneling is overcome. After that the current reflects RT of one electron (at a time) through the laterally quantized well states; the positions of the current peaks display systematic shifts and crossings with $B$, which reflect the magnetic field dependence of the energy of the well states *(15)*. In the negative bias, the response is very different, as expected. The current steps, rather than peaks, are observed in this polarity, as it should be when the tunneling

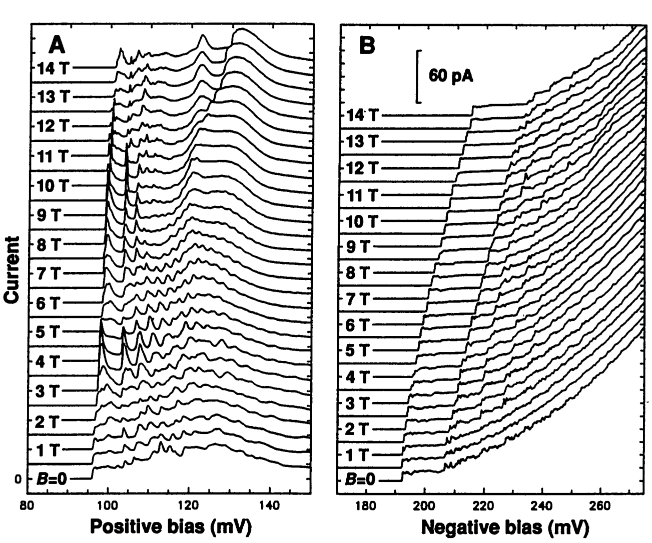

**Fig. 4.** Magnetotunneling data ($B$ perpendicular to the barriers) at 20 mK. The curves were taken every 0.5 T and are offset vertically by 15 pA. The shift of the first step to higher bias is due, in part, to the $1/2\hbar\omega_c$ diamagnetic shift of the lowest well state to a higher energy.

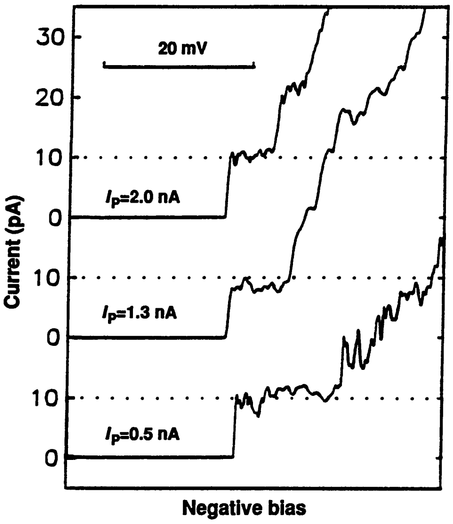

**Fig. 5.** Current-voltage curves of several devices made from the same heterostructure wafer; $I_p$ gives the value of the peak current, which is a measure of the "electrical size" of a device.

current is limited by the single-electron charging effects. This "Coulomb staircase" behavior is seen better in the magnetotunneling data because $B$ suppresses the short period (~1 mV) modulation. Steps corresponding to from one to six or seven electrons dynamically stored in the well are visible in the data of Fig. 4B.

The calculated values of $I^{(1)}$ are $I^{(1)+} \approx 4$ pA and $I^{(1)-} \approx 11$ pA in the positive and negative polarity, respectively. The experimental values, obtained from the first steps of several devices (Figs. 2 and 5), are $2I^{(1)+} = 9 \pm 2$ pA and $I^{(1)-} = 9.5 \pm 1$ pA; the agreement with the calculated values is very good because the transmission coefficients were obtained by fitting data of a large-area device. Moreover, in the negative bias $T_E > > T_C$ and we can estimate $I^{(1)-}$ as simply the current due to one electron tunneling every $\tau_W \approx \hbar/T_C E_0$: $I^{(1)-} = e/\tau_W \approx 14$ pA, which is also in good agreement with experiment. From the voltage extent of the steps in the negative bias and from fitting of current peaks in the positive bias (*16*) we obtain values of $U_C \approx 20$ K and $\delta E \approx 40$ K that are consistent with the observed temperature dependencies (for example, Fig. 3). Also, the sharpness of the rising current steps [0.2 mV, corresponding to 0.05 meV; see inset in Fig. 2C] is in itself strong evidence for a many-body component (such as $U_C$) in the tunneling-inhibiting potential, since it is not subject to various broadening mechanisms.

There are three major differences between SET in metal double junctions and in submicrometer DBRTS. First and most obvious is that Coulomb blockade is masked in DBRTS by a large threshold bias $V_{th} \sim 2E_0/e$ needed to align the states in the well with the emitter Fermi energy. Second, the size quantization of the well states in DBRTS coexists with the SET charging so that the two effects may be difficult to separate in measured *I-V* curves. Third, there are no electrons in the well at biases $V < V_{th}$ (zero current), unlike the case of experiments in (*1–4*). This effect is important because the charging energy of addition of the second electron involves two-electron repulsion in the well (*17*) and is greater than $U_C$ for the first electron (*18*).

## REFERENCES AND NOTES

1. T. A. Fulton and G. J. Dolan, *Phys. Rev. Lett.* **59**, 109 (1987); L. S. Kuzmin and K. K. Likharev, *JETP Lett.* **45**, 494 (1987); J. B. Barner and S. T. Ruggiero, *Phys. Rev. Lett.* **59**, 807 (1987).
2. C. J. Gorter, *Physica* **17**, 777 (1951); I. Giaever and H. R. Zeller, *Phys. Rev. Lett.* **20**, 1504 (1968).
3. For a review, see D. V. Averin and K. K. Likharev, in *Mesoscopic Phenomena in Solids*, B. L. Altshuler, P. A. Lee, R. B. Webb, Eds. (Elsevier, Amsterdam, 1991).
4. J. H. F. Scott-Thomas, S. B. Field, M. A. Kastner, H. I. Smith, D. A. Antoniadis, *Phys. Rev. Lett.* **62**, 583 (1989); L. P. Kouwenhoven, B. J. van Wees, K. J. P. M. Harmans, J. G. Williamson, *Surf. Sci.* **229**, 290 (1990); U. Meirav, M. A. Kastner, S. J. Wind, *Phys. Rev. Lett.* **65**, 771 (1990).
5. H. van Houten and C. W. J. Beenakker, *Phys. Rev. Lett.* **63**, 1893 (1989); Y. Meir, N. S. Wingreen, P. A. Lee, *ibid.* **66**, 3048 (1991).
6. See, for example, K. Kash *et al.*, *Appl. Phys. Lett.* **49**, 1043 (1986).
7. M. A. Reed *et al.*, *Phys. Rev. Lett.* **60**, 535 (1988).
8. M. Tewordt *et al.*, *J. Phys. Condens. Matter* **2**, 8969 (1990); S. Tarucha and Y. Hirayama, *Phys. Rev. B* **43**, 9373 (1991); M. W. Dellow *et al.*, *Electron. Lett.* **27**, 134 (1991).
9. B. Su, V. J. Goldman, M. Santos, M. Shayegan, *Appl. Phys. Lett.* **58**, 747 (1991).
10. V. J. Goldman, D. C. Tsui, J. E. Cunningham, *Phys. Rev. B* **35**, 9387 (1987); *Phys. Rev. Lett.* **58**, 1256 (1987).
11. A. N. Korotkov, D. V. Averin, K. K. Likharev, *Physica B* **165&166**, 927 (1990); L. I. Glazman and K. A. Matveev, *JETP Lett.* **51**, 484 (1990); A. Groshev, *Phys. Rev. B* **42**, 5895 (1990).
12. V. J. Goldman, D. C. Tsui, J. E. Cunningham, *Solid State Electron.* **31**, 731 (1988); A. Zaslavsky, V. J. Goldman, D. C. Tsui, J. E. Cunningham, *Appl. Phys. Lett.* **53**, 1408 (1988).
13. $C_W = C_E + C_C$. For the device shown in Figs. 2 to 4 at $V = -200$ mV we estimate $C_E \approx 3 \times 10^{-17}$ F and $C_C \approx 2 \times 10^{-17}$ F.
14. R. Landauer, *Philos. Mag.* **21**, 863 (1970).
15. C. G. Darwin, *Proc. Cambridge Philos. Soc.* **27**, 86 (1930).
16. B. Su, V. J. Goldman, J. E. Cunningham, in preparation.
17. G. W. Bryant, *Phys. Rev. Lett.* **59**, 1140 (1987).
18. V. J. Goldman, B. Su, J. E. Cunningham, in *Proceedings of the International Symposium on Nanostructures and Mesoscopic Systems*, W. P. Kirk and M. A. Reed, Eds. (Academic Press, New York, 1991).
19. We are grateful to J. E. Lukens for use of electron beam lithography facility and M. Shayegan for DBRTS material used in initial stages of this work (*9*). Supported in part by an Alfred P. Sloan Research Fellowship.

26 September 1991; accepted 9 December 1991

---

# Gas-Phase Rates of Alkane C–H Oxidative Addition to a Transient CpRh(CO) Complex

ERIC P. WASSERMAN, C. BRADLEY MOORE,* ROBERT G. BERGMAN*

**The gas-phase irradiation of $CpRh(CO)_2$ (Cp = $\eta^5$-$C_5H_5$) was examined in order to study the rates of reaction of the 16-electron intermediates presumed to be involved in the C–H oxidative addition of alkanes. "Naked" (unsolvated) CpRh(CO) was detected, and direct measurements of the rates of reaction of this very short-lived complex with alkane C–H bonds were made. Activation of C–H bonds occurs on almost every collision for alkanes of moderate size, and intermediates in which the alkanes are bound to the metal centers, without their C–H bonds being fully broken, are implicated as intermediates in the overall reaction.**

"UNACTIVATED" CARBON-HYDROGEN bonds, of the type present in alkanes, are among the strongest single bonds known. Because alkanes and alkyl chains make up a large percentage of natural materials, there is an incentive to develop methods for converting these unactivated C–H bonds into more reactive, and therefore useful, organic functional groups.

Activation of C–H bonds occurs readily on metal surfaces. There are also several known biological systems (such as cytochrome P-450 and methane monooxygenase) that contain metal complexes at their active sites that are capable of selectively activating C–H bonds. Some of these reactions undoubtedly proceed by free radical mechanisms, but it has been thought for some time that others are initiated by insertion of a metal center into the C–H linkage of the alkane R–H in a so-called "oxidative addition reaction." This leads to a hydrido(alkyl)metal complex, R–M–H, as shown in Eq. 1.

$$M + R\text{–}H \rightarrow R\text{–}M\text{–}H \qquad (1)$$

Several years ago we and others (*1, 2*) discovered a group of well-characterized hydrocarbon-soluble organometallic complexes capable of effecting the intermolecular oxidative addition or "C–H bond activation" reaction illustrated in Eq. 1 with sim-

---

Materials and Chemical Sciences Division, Lawrence Berkeley Laboratory, and the Department of Chemistry, University of California, Berkeley, CA 94720.

*To whom correspondence should be addressed.